Supplement of Earth Syst. Dynam., 12, 709–723, 2021
https://doi.org/10.5194/esd-12-709-2021-supplement

Earth System Dynamics
Open Access
EGU

Supplement of

Bayesian estimation of Earth's climate sensitivity and transient climate response from observational warming and heat content datasets

Philip Goodwin and B. B. Cael

Correspondence to: Philip Goodwin (p.a.goodwin@soton.ac.uk)

Supplementary Text

S1 On priors and updates to the WASP model

The WASP model described in Goodwin (2018) is used here, with updated prior distributions, functional forms of radiative forcing from greenhouse gasses and aerosols and internal noise in the energy imbalance. The time-step in the WASP model is altered from 48 time-steps per year in Goodwin (2018) to 12 time-steps per year here. The random-normal prior distribution for the Planck feedback, λ_{Planck} (Supplementary Table S1), is estimated via $\lambda_{Planck} = 4f\sigma T^3$, where f is the greenhouse fraction of upwards longwave radiation at the top of the atmosphere relative to the surface (Trenberth et al., 2014), σ is the Stephan-Boltzmann constant and T is the global mean surface temperature of Earth (Jones and Hapham, 2013). Uniform prior probability distributions for λ_{fast} (from -3.0 to +1.0 $Wm^{-2}K^{-1}$) and λ_{slow} (from -3.0 to +3.0 $Wm^{-2}K^{-1}$) are used.

The random-normal prior distribution for the CO_2 radiative forcing coefficient (Supplementary Table S1) is taken from the estimate of IPCC (2013), $a_{CO2} = 5.35 \pm 0.27$ Wm^{-2}. The functional forms of radiative forcing from CH_4 and N_2O are updated after Etminan et al. (2016), with random-normal prior distributions of uncertainty (Supplementary Table S1) to reflect uncertainty for these relations estimated in Etminan et al. (2016). A radiative forcing term is introduced to WASP here to represent the internal variability in Earth's energy imbalance using AR1 noise, with the constants tuned to imposed monthly and annual root-mean-square energy imbalance after Trenberth et al. (2014).

S2 Radiative forcing from aerosols in the WASP model

The calculation of radiative forcing from aerosols in the WASP model (Goodwin, 2016) is updated in this study. The version of WASP described in Goodwin (2018) uses a single time series for aerosol radiative forcing scaled by a single uncertainty parameter that is varied between ensemble members. Here, aerosol radiative forcing is separated into direct and indirect aerosol forcing components from emissions of different types of aerosols: Black Carbon (BC), Organic Carbon (OC), sulphates (SO_x), nitrous oxides (NO_X), ammonia (NH_3) and volatile organic compounds (VOC).

The version of WASP used here is updated to employ aerosol radiative forcing based on the FAIR v1.3 (Smith et al., 2018) model scheme, with this scheme chosen as it avoids the use of iterative computational methods and thus retains computational efficiency. The direct aerosol radiative forcing over time is related to the emissions of different anthropogenic aerosol types, E_x, via

$$R_{dir-aero}(t) = \gamma_{aero-BC}E_{BC} + \gamma_{aero-OC}E_{OC} + \gamma_{aero-SO_x}E_{SO_x} + \gamma_{aero-NO_x}E_{NO_x} + \gamma_{aero-NH_3}E_{NH_3} + \gamma_{aero-VOC}E_{VOC} \quad \text{(S1)}$$

which assumes anthropogenic aerosol are sufficiently short-lived in the atmosphere such that radiative forcing can be related directly to emissions without an intermediate step of calculating atmospheric concentrations (Smith et al., 2018).

The AeroCom experiments (Myhre et al., 2013) analyse direct radiative forcing for each aerosol type across multiple atmospheric models in the year 2010. Smith et al. (2018) uses these 2010 best estimates (Myhre et al., 2013) to constrain the coefficients $\gamma_{aero-BC}$, $\gamma_{aero-OC}$, $\gamma_{aero-SO_x}$, $\gamma_{aero-NO_x}$, $\gamma_{aero-NH_3}$ and $\gamma_{aero-SOA}$ in the FaIR model. In the WASP model used here, this is extended by using the uncertainty estimates in Myhre et al. (2013) to independently vary the values of coefficients $\gamma_{aero-BC}$, $\gamma_{aero-OC}$, $\gamma_{aero-SO_x}$, $\gamma_{aero-NO_x}$, $\gamma_{aero-NH_3}$ and $\gamma_{aero-VOC}$ between the prior ensemble members (Supplementary Table S1). Thus, the prior WASP ensemble here is representative of the multi-model variation in how sensitive direct aerosol radiative forcing is to emissions of each aerosol type evaluated in Myhre et al. (2013).

The coefficients relating aerosol emissions to direct radiative forcing are thus written (Supplementary Table S1): $\gamma_{aero-SO_x} = (-0.32 \pm 0.11)/E_{SO_x-2010}$; $\gamma_{aero-BC} = (0.18 \pm 0.07)/E_{BC-2010}$; $\gamma_{aero-OC} = (-0.03 \pm 0.01)/E_{OC-2010}$; and $\gamma_{aero-VOC} = (-0.06 \pm 0.09)/E_{VOC-2010}$. Nitrate aerosol radiative forcing is split into components of 40% from NO_X and 60% from NH_3, as used by Smith et al. (2018), giving: $\gamma_{NO_x} = 0.4 \times (-0.08 \pm 0.04)/E_{NO_x-2010}$; and $\gamma_{NH_3} = 0.6 \times (-0.08 \pm 0.04)/E_{NH_3-2010}$.

WASP is also updated to use an emulation of indirect aerosol radiative forcing from aerosol-cloud interaction, $R_{aci}(t)$ in Wm^{-2}, after FaIRv1.3 model (Smith et al., 2018),

$$R_{aci}(t) = R_{aci:2011}\frac{G(t) - G(t_{1765})}{G(t_{2011}) - G(t_{1765})} \quad \text{(S2)}$$

where $R_{aci:2011}$ is the radiative forcing from aerosol cloud interaction in 2011, and G is related to emissions of aerosol components via;

$$G(t) = -1.95\log\left(1 + 0.0111E_{SO_x}(t) + 0.0139[E_{OC}(t) + E_{BC}(t)]\right) \quad \text{(S3)}$$

We vary the value of $R_{aci:2011}$ between the prior ensemble members to account for the skewed uncertainty in indirect aerosol radiative forcing estimated within IPCC AR5 (IPCC, 2013). To account for a skew in the uncertainty in historic indirect aerosol radiative forcing (IPCC, 2013), a skewed-normal prior distribution for $R_{aci:2011}$ is adopted (Supplementary Table S1).

S3 Time-evolving climate sensitivity in the WASP model

The WASP model code considers feedback processes evolving over time independently to different sources of radiative forcing. This supplementary section explores how one single feedback process evolves over time to a single source of radiative forcing in WASP. For an idealised step function of radiative forcing occurring at $t = t_0$, the climate feedback contribution from a given process is assumed to start at $\lambda(t_0) = 0$ at the moment of the step function, and then approach the equilibrium value for that process over an e-folding timescale τ,

$$\lambda(t) = \lambda_{equil}\left(1 - \exp\frac{-(t - t_0)}{\tau}\right) \tag{S4}$$

This relationship (S4) is equivalently expressed relative to the value of λ at some intermediate time t_1,

$$\lambda(t) = \lambda(t_1) + \left(\lambda_{equil} - \lambda(t_1)\right)\left(1 - \exp\frac{-(t - t_1)}{\tau}\right) \tag{S5}$$

The value of $\lambda(t)$ is complicated when the magnitude of radiative forcing continues to rise after the initial perturbation, since now each contribution to the rise in radiative forcing will contribute to $\lambda(t)$ via an exponential decay from 0 to λ_{equil} over a different time-interval relating to the length of time ago that that specific contribution to the rise in radiative forcing occurred. To calculate $\lambda(t)$ when there have been multiple contributions to the rise in magnitude of radiative forcing at different times we may write,

$$\lambda(t) = \int_{R'=0}^{R'=R(t)} \lambda_{equil}\left(1 - \exp\frac{-(t - t')}{\tau}\right) dR' \Big/ \int_{R'=0}^{R'=R(t)} dR' \tag{S6}$$

where t_0 is the most recent time that R has changed sign such that $R(t_0) = 0$; $R = R'$ at $t = t'$; and it is assumed that R has been either unchanging or increasing in magnitude for all time since t_0 (i.e. $[dR/dt]/R > 0$). This integral may be re-written for a numerical time-stepping model as a summation over all timesteps t' since the most recent time that R changed sign,

$$\lambda(t) = \sum \lambda_{equil}\left(1 - \exp\frac{-(t - t')}{\tau}\right)\delta R(t') \Big/ \sum \delta R(t') \tag{S7}$$

where $\delta R(t')$ is the increase in radiative forcing at time-step t'. However, numerically solving this integral via the summation (S7) would require a numerical model to take many steps in the calculation, recall many values of past radiative forcing and utilise an algorithm to identify the most recent time when R changed

sign. To simplify and speed up the calculation, WASP adopts an approximation that requires knowledge of only the previous time-step value of climate feedback from that process, $\lambda(t-\delta t)$, and the previous timestep value of radiative forcing, $R(t-\delta t)$, and the additional radiative forcing for the current timestep, δR.

If the magnitude of R has not increased since the previous time-step, $\delta R/R(t-\delta t) \leq 0$, a time-step equation of the same form as (S5) is applied:

$$\lambda(t) = \lambda(t-\delta t) + \left(\lambda_{equil} - \lambda(t-\delta t)\right)\left(1 - \exp\frac{-\delta t}{\tau}\right) \tag{S8}$$

If the magnitude of R has increased since the last time-step, $\delta R/R(t-\delta t) > 0$, then we have a summation of λ from two components of radiative forcing, weighted by their respective relative contributions to radiative forcing as per (S7): the λ value for radiative forcing existing at the previous timestep plus the value for the radiative forcing since the last time-step. Considering (S7) and (S8) we write,

$$\lambda(t) = \frac{\left(\lambda(t-\delta t) + \left(\lambda_{equil} - \lambda(t-\delta t)\right)\left(1 - \exp\frac{-\delta t}{\tau}\right)\right)R(t-\delta t) + \left(\lambda_{equil}\left(1 - \exp\frac{0}{\tau}\right)\right)\delta R}{R(t-\delta t) + \delta R} \tag{S9}$$

Noting that $\left(1 - \exp\frac{0}{\tau}\right) = 0$, and $R(t) = R(t-\delta t) + \delta R$, this summation (S9) simplifies to,

$$\lambda(t) = \left|\frac{R(t-\delta t)}{R(t)}\right|\left[\lambda(t-\delta t) + \left(\lambda_{equil} - \lambda(t-\delta t)\right)\left(1 - \exp\frac{-\delta t}{\tau}\right)\right] \tag{S10}$$

Supplementary Figure S7 shows this numerical scheme (eqns. S8 and S10) applied to two idealised step-function scenarios in radiative forcing for a system with Planck, fast and multidecadal feedbacks each separately calculated using eqns. (S8) and (S10). For the single step-function scenario (Figure S7a) the fast and multidecadal feedback responses begin at 0 and continually increase in magnitude over their respective timescales (Figure 7b), with the overall feedback response evolving accordingly (Figure 7c). However, for the double-step function scenario (Figure 7d) the responses are altered, with both fast and multidecadal feedbacks reducing when the second step-function in radiative forcing is applied (Figure 7e,f) before evolving towards their equilibrium values afterwards.

S4 The observational constraints to select posterior ensembles

The WASP model selects prior ensemble members for inclusion into a posterior ensemble via comparison with observational constraints (Supplementary Table 2). These constraints include reconstructions of historical: Global mean surface temperature (HadCRUT5 or HadCRUT5 (no infill) in Supplementary Table S2); ocean heat content for depth layers or the whole ocean (Cheng et al. or NODC in Supplementary Table S2); global sea surface temperature anomaly (HadSST4 in Supplementary Table S2); and global ocean carbon uptake (The Global Carbon Budget in Supplementary Table S2).

The WASP model contains one input parameter for the ratio of global sea-surface warming to global mean surface warming at equilibrium (Ratio 1 or r_1 in Supplementary Table S1) and another for the ratio of global whole-ocean warming to global sea-surface warming at equilibrium (Ratio 2 or r_2 in Supplementary Table S1). It is these input parameters that require the use of a separate observational constraint for sea surface temperatures (HadSST4 in Supplementary Table S2) and an observational constraint for ocean carbon uptake (The Global Carbon Budget in Supplementary Table S2) to be applied. As the r_1 parameter is varied between prior ensemble members, simulated global mean surface warming and sea surface temperature warming vary differently (relative to each other) across the ensemble. Therefore, the observational constraints for both global surface temperature and sea surface temperature are required to help constrain the posterior values of r_1 within the posterior ensembles. As the r_2 parameter is varied between prior ensemble members, the relative ocean uptakes of heat and carbon are varied across the ensemble members. Therefore, observational constraints for both ocean heat and carbon uptake are required to constrain the values of r_2 in the posterior ensembles.

Supplementary References

Andrews T., Gregory J.M., Webb M.J.: The dependence of radiative forcing and feedback on evolving patterns of surface temperature change in climate models. J Clim 28:1630–1648. https://doi.org/10.1175/JCLI-D-14-00545.1, 2015.

Cheng, L., Trenberth, K.E., Fasullo, J., Boyer, T., Abraham, J., Zhu, J.: Improved estimates of ocean heat content from 1960 to 2015. Science Advances, 3, 3, e1601545, https://doi.org/10.1126/sciadv.1601545, 2017.

Etminan, M., Myhre, G., Highwood, E.J., Shine, K.P.: Radiative forcing of carbon dioxide, methane, and nitrous oxide: A significant revision of the methane radiative forcing, Geophys. Res. Lett., 43, 12,614–12,623, https://doi:10.1002/2016GL071930, 2016.

Fine, R. A., Peacock, S., Maltrud, M. E., & Bryan, F. O.: A new look at ocean ventilation time scales and their uncertainties. Journal of Geophysical Research: Oceans, 122, 3771–3798. https://doi.org/10.1002/2016JC012529, 2017.

Goodwin, P.: On the time evolution of climate sensitivity and future warming. Earth's Future 6, EFT2466, https://doi.org/10.1029/2018EF000889, 2018.

Gregory, J.M., Andrews, T., Good, P., Mauritsen, T., Forster, P.M.: Small global-mean cooling due to volcanic radiative forcing. Climate Dynamics, 47, 3979-3991, https://doi.org/10.1007/s00382-016-3055-1, 2016.

IPCC: Climate Change 2013: The Physical Science Basis. Contribution of Working Group 1 to the Fifth Assessment Report of the Intergovernmental Panel on Climate Change In T. F. Stocker, et al. (Eds.). (1535 pp.). Cambridge, UK: Cambridge University Press. https://doi.org/10.1017/CBO9781107415324, 2013.

Jones, P. D., Harpham, C., Estimation of the absolute surface air temperature of the Earth. J. Geophys. Res. Atmos., 118, 3213–3217, https://doi.org/10.1002/jgrd.50359, 2013.

Kennedy, J. J., Rayner, N. A., Atkinson, C. P., and Killick, R. E.: An ensemble data set of sea-surface temperature change from 1850: the Met Office Hadley Centre HadSST.4.0.0.0 data set. Journal of Geophysical Research: Atmospheres, 124. https://doi.org/10.1029/2018JD029867, 2019.

le Quéré, C., Andrew, R. M., Friedlingstein, P., Sitch, S., Hauck, J., Pongratz, J., Pickers, P. A., Korsbakken, J. I., Peters, G. P., Canadell, J. G., Arneth, A., Arora, V. K., Barbero, L., Bastos, A., Bopp, L., Chevallier, F., Chini, L. P., Ciais, P., Doney, S. C., Gkritzalis, T., Goll, D. S., Harris, I., Haverd, V., Hoffman, F. M., Hoppema, M., Houghton, R. A., Hurtt, G., Ilyina, T., Jain, A. K., Johannessen, T., Jones, C. D., Kato, E., Keeling, R. F., Goldewijk, K. K., Landschützer, P., Lefèvre, N., Lienert, S., Liu, Z., Lombardozzi, D., Metzl, N., Munro, D. R., Nabel, J. E. M. S., Nakaoka, S., Neill, C., Olsen, A., Ono, T., Patra, P., Peregon, A., Peters, W., Peylin, P., Pfeil, B., Pierrot, D., Poulter, B., Rehder, G., Resplandy, L., Robertson, E., Rocher, M., Rödenbeck, C., Schuster, U., Schwinger, J., Séférian, R., Skjelvan, I., Steinhoff, T., Sutton, A., Tans, P. P., Tian, H., Tilbrook, B., Tubiello, F. N., van der Laan-Luijkx, I. T., van der Werf, G. R., Viovy, N., Walker, A. P., Wiltshire, A. J., Wright, R., Zaehle, S., and Zheng, B.: Global Carbon Budget 2018, Earth Syst. Sci. Data, 10, 2141–2194, https://doi.org/10.5194/essd-10-2141-2018, 2018.

Levitus, S., Antonov, J.I., Boyer, T.P., Baranova, O.K., Garcia, H.E., Locarnini, R.A., Mishonov, A.V., Reagan, J.R., Seidov, D., Yarosh, E.S. and Zweng, M.M.: World ocean heat content and thermosteric sea levelchange (0–2000 m), 1955–2010. Geophysical Research Letters, 39, https://doi.org/10.1029/2012GL051106, 2012.

Morice, C.P., Kennedy, J.J., Rayner, N.A., Winn, J.P., Hogan, E., Killick, R.E., Dunn, R.J.H., Osborn, T.J., Jones, P.D., and Simpson, I.R.: An updated assessment of near-surface temperature change from 1850: the HadCRUT5 dataset. Journal of Geophysical Research. http://doi.org/10.1029/2019JD0323611, 2021

Myhre, G., Samset, B. H., Schulz, M., Balkanski, Y., Bauer, S., Berntsen, T. K., Bian, H., Bellouin, N., Chin, M., Diehl, T., Easter, R. C., Feichter, J., Ghan, S. J., Hauglustaine, D., Iversen, T., Kinne, S., Kirkevåg, A., Lamarque, J.-F., Lin, G., Liu, X., Lund, M. T., Luo, G., Ma, X., van Noije, T., Penner, J. E., Rasch, P. J., Ruiz, A., Seland, Ø., Skeie, R. B., Stier, P., Takemura, T., Tsigaridis, K., Wang, P., Wang, Z., Xu, L., Yu, H., Yu, F., Yoon, J.-H., Zhang, K., Zhang, H., and Zhou, C.: Radiative forcing of the direct aerosol effect from AeroCom Phase II simulations, Atmos. Chem. Phys., 13, 1853–1877, https://doi.org/10.5194/acp-13-1853-2013, 2013.

Trenberth, K.E., Fasullo, J.T., and Balmaseda, M.A.: Earth's Energy Imbalance, Journal of Climate, 27, 3129-3144. https://doi.org/10.1175/JCLI-D-13-00294.1, 2014.

van der Ent, R. J., Tuinenburg, O. A.: The residence time of water in the atmosphere revisited. Hydrology and Earth System Sciences, 21, 779–790. https://doi.org/10.5194/hess-21-779-2017, 2017.

Supplementary Tables:

Model input parameter	**Prior Distribution**	**Notes**
λ_{Planck}, Planck climate feedback	Normal, μ= 3.2 Wm^{-2}; σ = 0.2 Wm^{-2}	Estimated from global energy budget (Trenberth et al., 2014) and global mean temperature (Jones and Harpham, 2013).
λ_{fast}^{equil}, climate feedback from fast processes at equilibrium	Uniform, min. = -3.0 Wm^{-2}, max. = +1.0 Wm^{-2}	Assume equal prior likelihood from -3.0 to +1.0 Wm^{-2}
τ_{fast}, e-folding timescale of fast climate feedback processes	Normal, μ =8.9 days , σ = 0.4 days	Set to residence timescale for water vapour in the atmosphere (van der Ent and Tuinenberg, 2017)
$\lambda_{multidecadal}^{equil}$, climate feedback from slow processes at equilibrium	Uniform, min. = -3.0 Wm^{-2}, max. = +3.0 Wm^{-2}.	Assume equal prior likelihood from -3.0 to +3.0 Wm^{-2}
$\tau_{multidecadal}$, e-folding timescale of slow climate feedback processes	Uniform, min. = 20 years, max. = 45 years	Linked to the minimum time window over which slow climate feedbacks are evaluated (20 years) in climate models by Andrews et al. (2015) and the ventilation timescale of the upper thermocline (45 years) identified by Fine et al. (2017).
a_{CO2}, the radiative forcing coefficient for a log change in CO_2	Normal, μ = 5.35 Wm^{-2}, σ = 0.27 Wm^{-2}	IPCC (2013)
Dimensionless uncertainty in N_2O radiative forcing	Normal, μ = 1.0, σ = 0.05.	To represent percentage uncertainty of Etminan et al. (2016)

Dimensionless uncertainty in CH_4 radiative forcing	Normal, μ = 1.0, σ = 0.07.	To represent percentage uncertainty of Etminan et al. (2016)
Dimensionless uncertainty in Halocarbon radiative forcing	Normal, μ = 1.0, σ = 0.05.	To represent percentage uncertainty of Myhre et al. (2013)
Coefficient of radiative forcing from volcanic aerosols	Normal, μ = -19.0 Wm^{-2}, σ = -0.5 Wm^{-2}.	Relates volcanic AOD to radiative forcing after Gregory et al. (2016)
Radiative forcing from SO_X aerosols in 2010, $\gamma_{SO_x}E_{SO_x}$	Normal, μ = -0.31 Wm^{-2}, σ = 0.11 Wm^{-2}	From AeroCom experiment, Myhre et al. (2013)
Radiative forcing from Black Carbon (BC) aerosols in 2010, $\gamma_{BC}E_{BC}$	Normal, μ = 0.18 Wm^{-2}, σ = 0.07 Wm^{-2}	From AeroCom experiment, Myhre et al. (2013)
Radiative forcing from Nitrous Oxide (NO_X) aerosols in 2010, $\gamma_{NO_x}E_{NO_x}$	Normal, μ = -0.032 Wm^{-2}, σ = 0.016 Wm^{-2}	From AeroCom experiment, Myhre et al. (2013) with 40% weighting
Radiative forcing from Volatile Organic Compound (NMVOC) aerosols in 2010, $\gamma_{SOA}E_{NMVOC}$	Normal, μ = -0.06 Wm^{-2}, σ = 0.09 Wm^{-2}	From AeroCom experiment, Myhre et al. (2013)
Radiative forcing from Organic Carbon (OC) aerosols in 2010, $\gamma_{OC}E_{OC}$	Normal, μ = -0.03 Wm^{-2}, σ = 0.01 Wm^{-2}	From AeroCom experiment, Myhre et al. (2013)
Radiative forcing from NH_3 aerosols in 2010, $\gamma_{NH_3}E_{NH_3}$	Normal, μ = -0.048 Wm^{-2}, σ = 0.024 Wm^{-2}	From AeroCom experiment, Myhre et al. (2013)
The radiative forcing from indirect aerosol effects in 2010, $-R_{aci:2011}$	Skew-normal, μ = -0.55 Wm^{-2}, σ = 0.37 Wm^{-2}, skew = -2.0.	To approximate indirect aerosol radiative forcing distribution of AR5 (IPCC., 2013).
Carbon exchange e-folding timescale between atmosphere and surface ocean mixed layer	Uniform, min. = 0.5 yrs, max. = 1.0 yrs	As used in WASP prior ensemble of Goodwin (2018).

Tracer exchange e-folding timescale surface ocean mixed layer to upper thermocline	Uniform, min. = 5 yrs, max. = 40 yrs	
Tracer exchange e-folding timescale surface ocean mixed layer to intermediate water	Uniform, min. = 15 yrs, max. = 60 yrs	
Tracer exchange e-folding timescale surface ocean mixed layer to deep water	Uniform, min. = 100 yrs, max. = 500 yrs	
Tracer exchange e-folding timescale surface ocean mixed layer to bottom water	Uniform, min. = 400 yrs, max. = 1500 yrs	
The atmosphere-ocean buffered carbon inventory, I_b	Uniform, min. = 3100 PgC, max. = 3500 PgC	
Ratio of surface warming global near surface to global sea surface at equilibrium, ratio 1 (r_1)	Uniform, min. = 0.20, max. = 1.5	
Ratio of global whole-ocean warming to global sea surface warming at equilibrium, ratio 2 (r_2)	Uniform, min. = 0.1, max. = 1.0	

Table S1: Prior distributions of the 25 varied model input parameters.

Historic observational constraint	**Mean and standard deviation of likelihood used for the ensembles**	
Surface warming anomalies, relative to 2000-2018	***HadCRUT5 ensembles***	***HadCRUT5 (no infill) ensemble***
ΔT during 1850-1899	μ = -0.973 °C; σ = 0.074 °C.	μ = -0.904 °C; σ = 0.096 °C.
ΔT during 1900-1919	μ = -1.042 °C; σ = 0.067 °C.	μ = -1.012 °C; σ = 0.081 °C.
ΔT during 1920-1939	μ = -0.820 °C; σ = 0.061 °C.	μ = -0.792 °C; σ = 0.073 °C.
ΔT during 1940-1959	μ = -0.666 °C; σ = 0.064 °C.	μ = -0.653 °C; σ = 0.076 °C.
ΔT during 1960-1979	μ = -0.706 °C; σ = 0.027 °C.	μ = -0.679 °C; σ = 0.049 °C.
ΔT during 1980-1999	μ = -0.374 °C; σ = 0.023 °C.	μ = -0.343 °C; σ = 0.048 °C.
SST anomaly relative to 1961-1990	***All ensembles*** **(HadSST4)**	
ΔSST during 1850-1899	μ = -0.281 °C, σ = 0.105 °C	
Heat content anomaly	***Cheng et al. ensembles***	***NODC ensemble***
ΔOHC upper 700m, 1960-1969 to 2006-2015	$\mu = 177.8\times10^{21}$ J; $\sigma = 13.8\times10^{21}$ J	-
ΔOHC from 700m to 2000m, 1960-1969 to 2006-2015	$\mu = 75.6\times10^{21}$ J; $\sigma = 12.3\times10^{21}$ J	-
ΔOHC for whole ocean, 1960-1969 to 2006-2015	$\mu = 360\times10^{21}$ J; $\sigma = 35\times10^{21}$ J	-
ΔOHC upper 700m, from 1955-1959 to 2015-2019	-	$\mu = 211.9\times10^{21}$ J; $\sigma = 18.5\times10^{21}$ J
ΔOHC upper 2000m, from 1955-1959 to 2015-2019	-	$\mu = 314.5\times10^{21}$ J; $\sigma = 20.3\times10^{21}$ J
Total Earth System heat content anomaly, 1971 to 2010	-	$\mu = 274\times10^{21}$ J; $\sigma = 48\times10^{21}$ J
Ocean carbon uptake	***All ensembles (Global Carbon Budget)***	

Whole ocean carbon content increase, 1982 to start of 2018	μ= 71.2 PgC, σ= 24.3 PgC

Table S2: Historic likelihood distributions applied as constraints to extract the posterior ensemble from the prior ensemble. Quantities are derived from observational-reconstruction datasets HadCRUT5 (Morice et al., 2019); HadCRUT5 (no infill); NODC (Levitus et al., 2012); Cheng et al. (2017); HadSST4 (Kennedy et al., 2019); and the Global Carbon Budget (le Quéré et al., 2018). The mean values (μ) for each multi-year average quantity (aside from NODC) are calculated as the time-average of the annual means for the relevant period. NODC already provides the 5-year time average. The standard deviation (σ) is provided by over the relevant 5-year time-period for the NODC dataset, while σ in the ocean carbon budget refers to an instantaneous cumulative change and is calculated from the 2 times the standard deviation of observation-constrained ocean models used within the Global Carbon Budget (le Quéré et al., 2018); where we multiply the standard deviation of the observation-constrained models by 2 since this small sample of 7 models may not be dispersive enough to capture the full uncertainty in ocean carbon uptake. For all other datasets where a multi-year time average is used, the value of σ for the time-average periods considered is estimated as the time-average of the annual values of σ. In the HadCRUT5 and HadCRUT5 (no infill) datasets the annual σ is assumed to be given by the annual 95% range in temperature anomaly divided by 4. This method of estimating the multi-year time-average from annual values of σ is equivalent to assuming perfect correlation between where the true value lies within the uncertainty distribution from one year to the next, and provides a larger value of σ for the relevant time-period than assumptions involving reduced correlation.

Supplementary Figures:

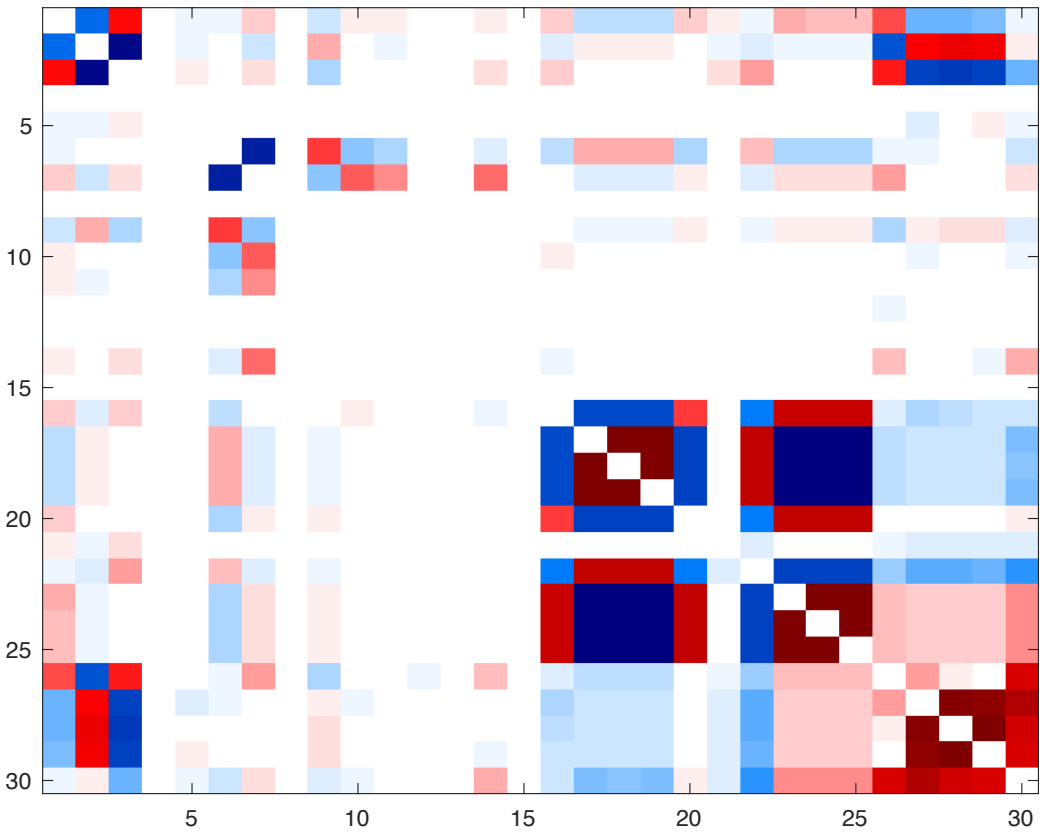

Figure S1: Correlations between model parameter posteriors and model outputs for the weighted metaensemble. Rows and columns 1-25 correspond to the parameters listed in Supplementary Figures S2-S6 in the order they appear in the x-axis of those figures (e.g. 1 is λ_{Planck}, 2 is λ_{fast}^{equil}, …); rows and columns 26-30 are ECS_{20}, ECS_{50}, ECS_{100} ECS_{140}, and TCR respectively. Red indicates positive correlation and blue indicates negative correlation.

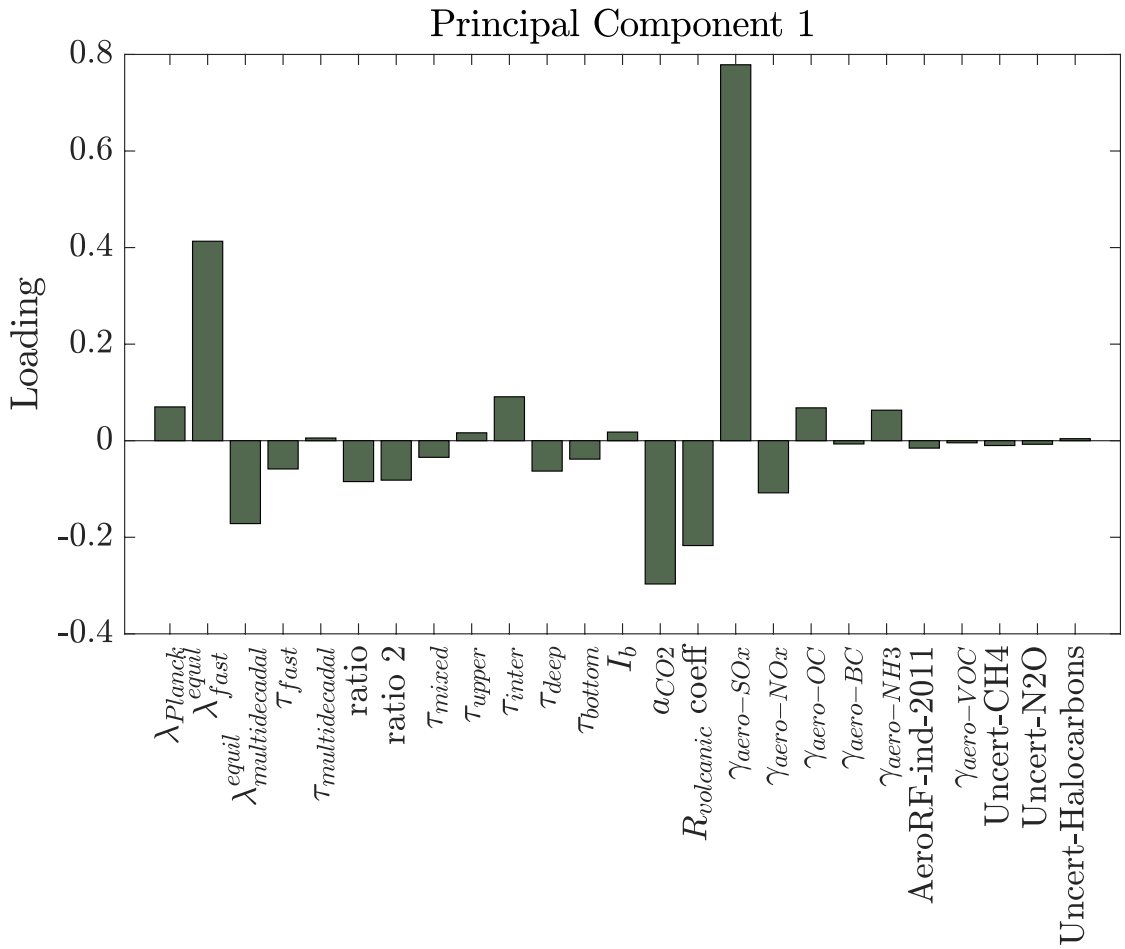

Figure S2. Principle component 1 of the varied model parameters within the posterior model ensembles.

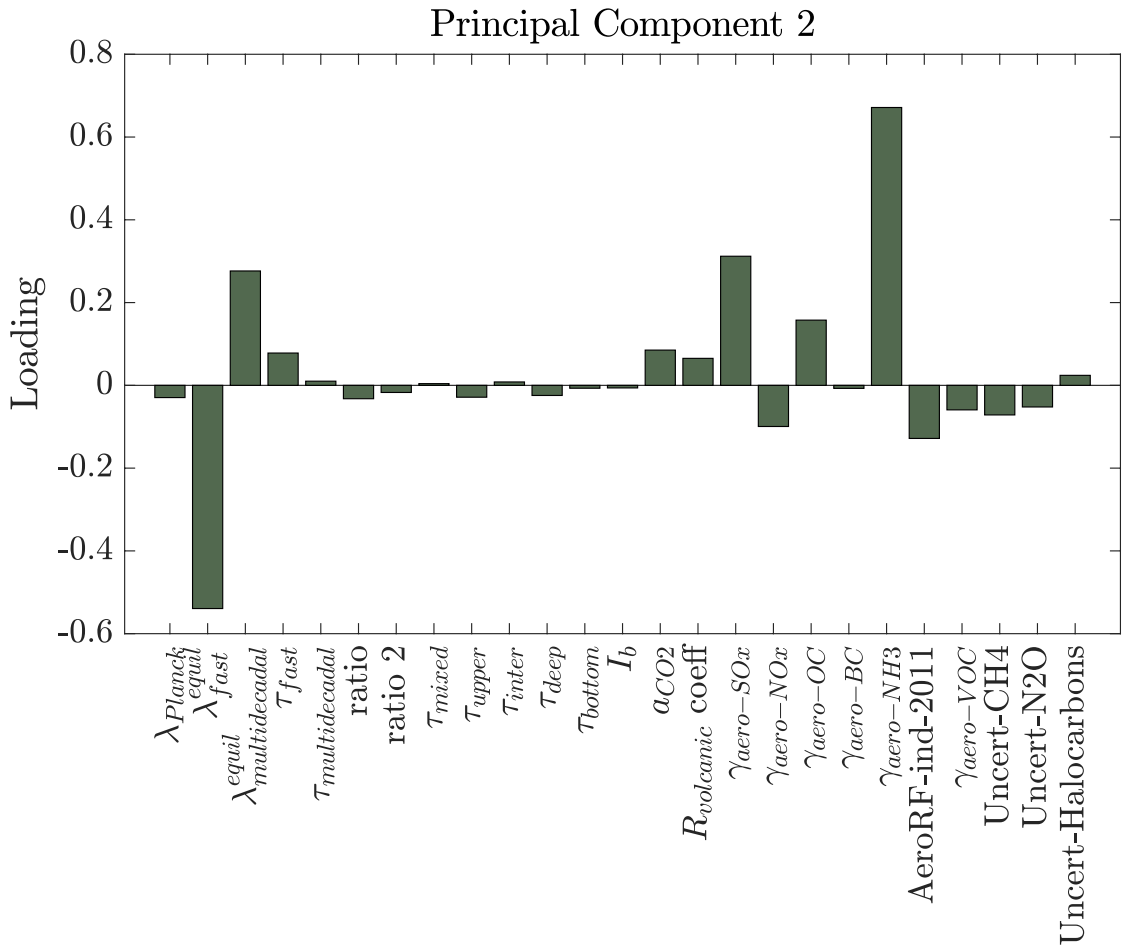

Figure S3. Principle Component 2 of the posterior model ensembles.

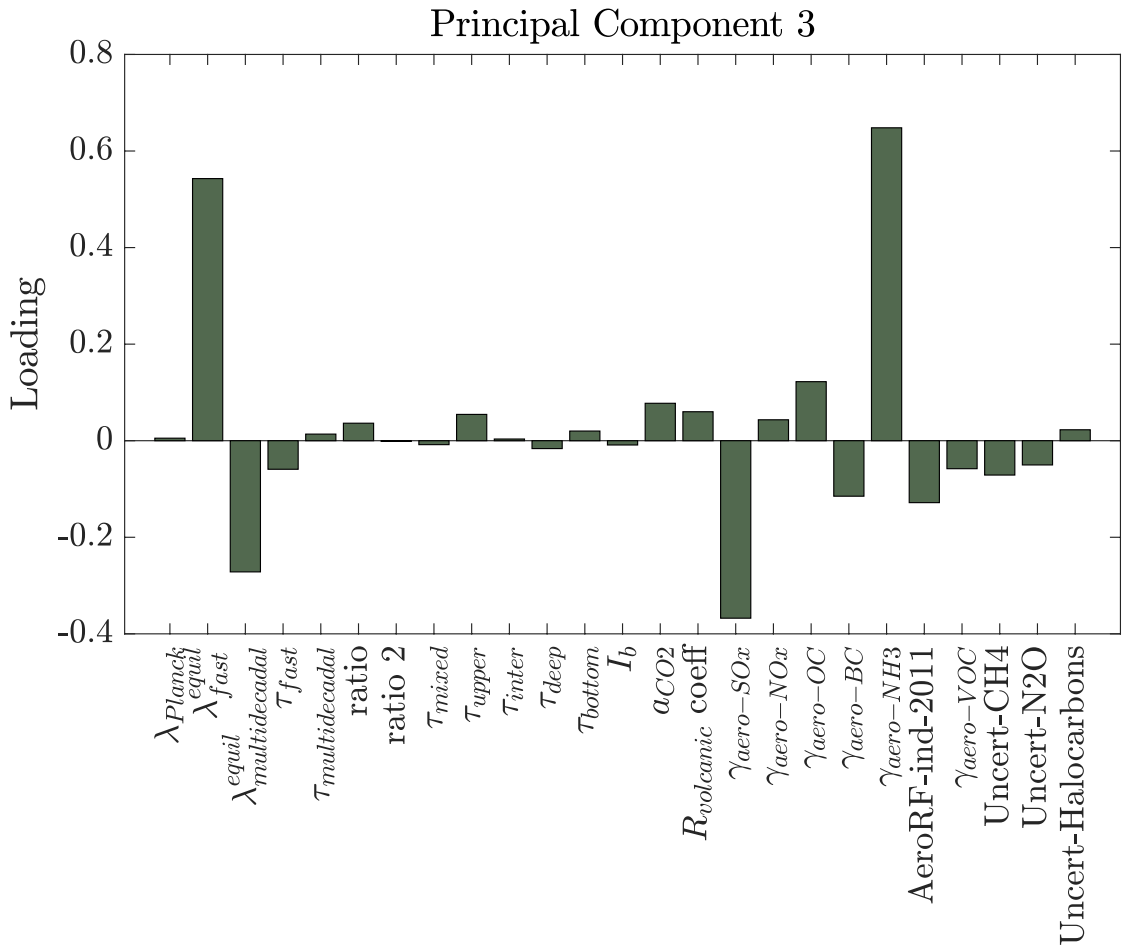

Figure S4. Principle Component 3 of the posterior model ensembles.

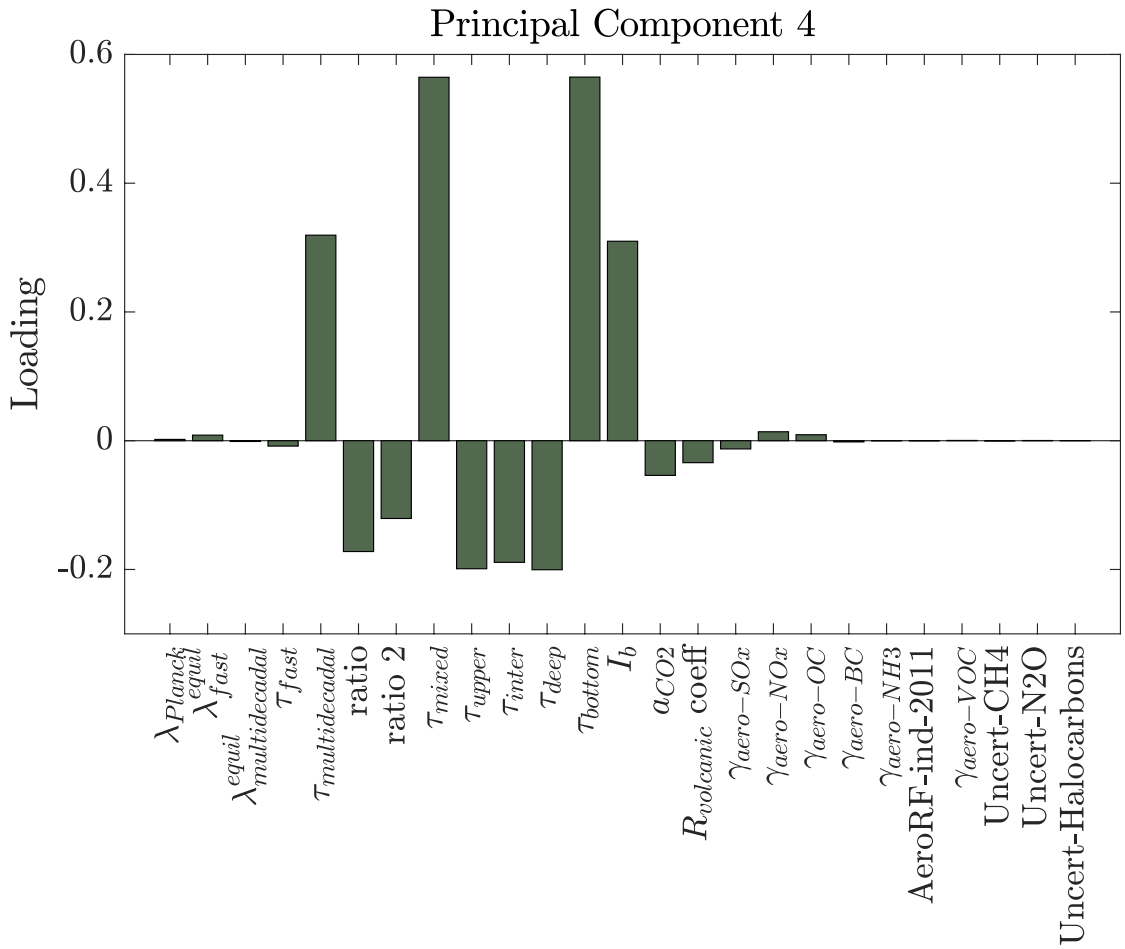

Figure S5. Principle Component 4 of the posterior model ensembles.

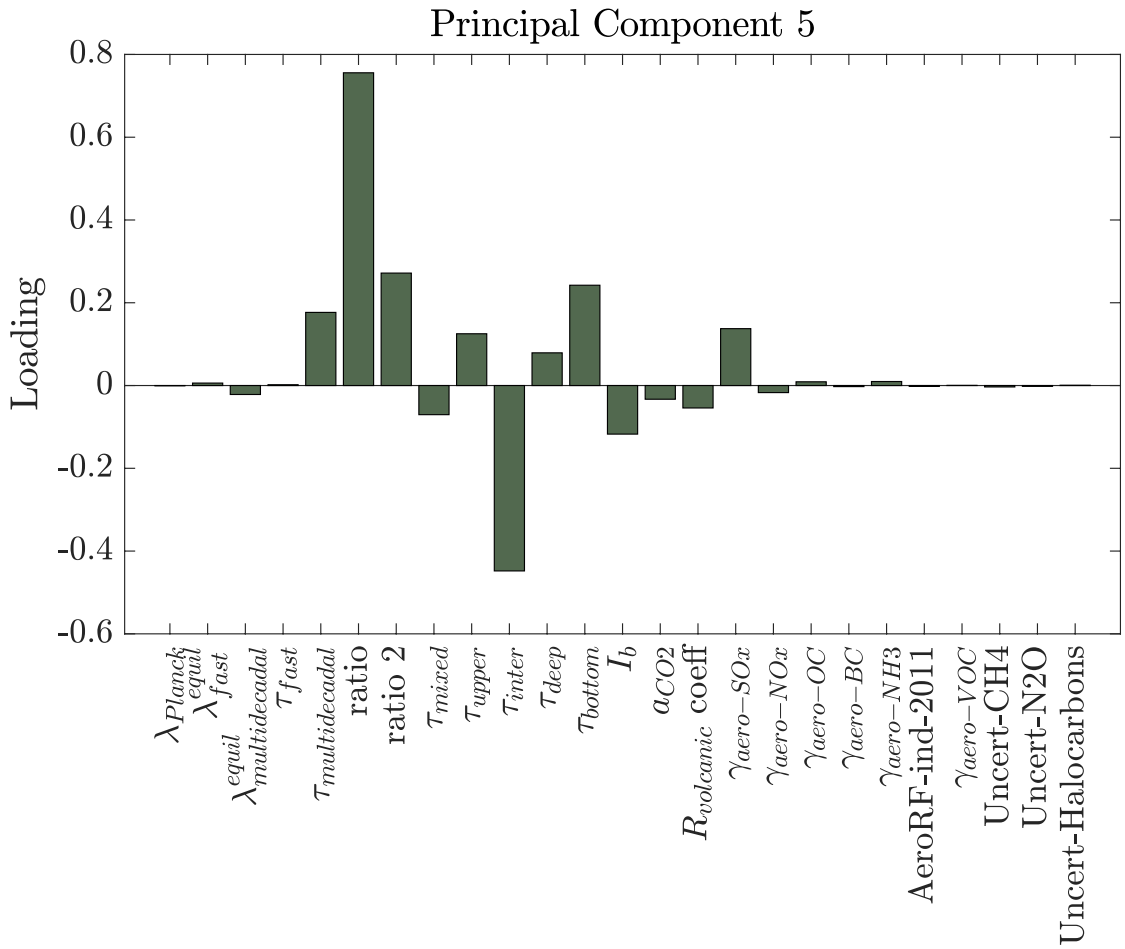

Figure S6. Principle Component 5 of the posterior model ensembles.

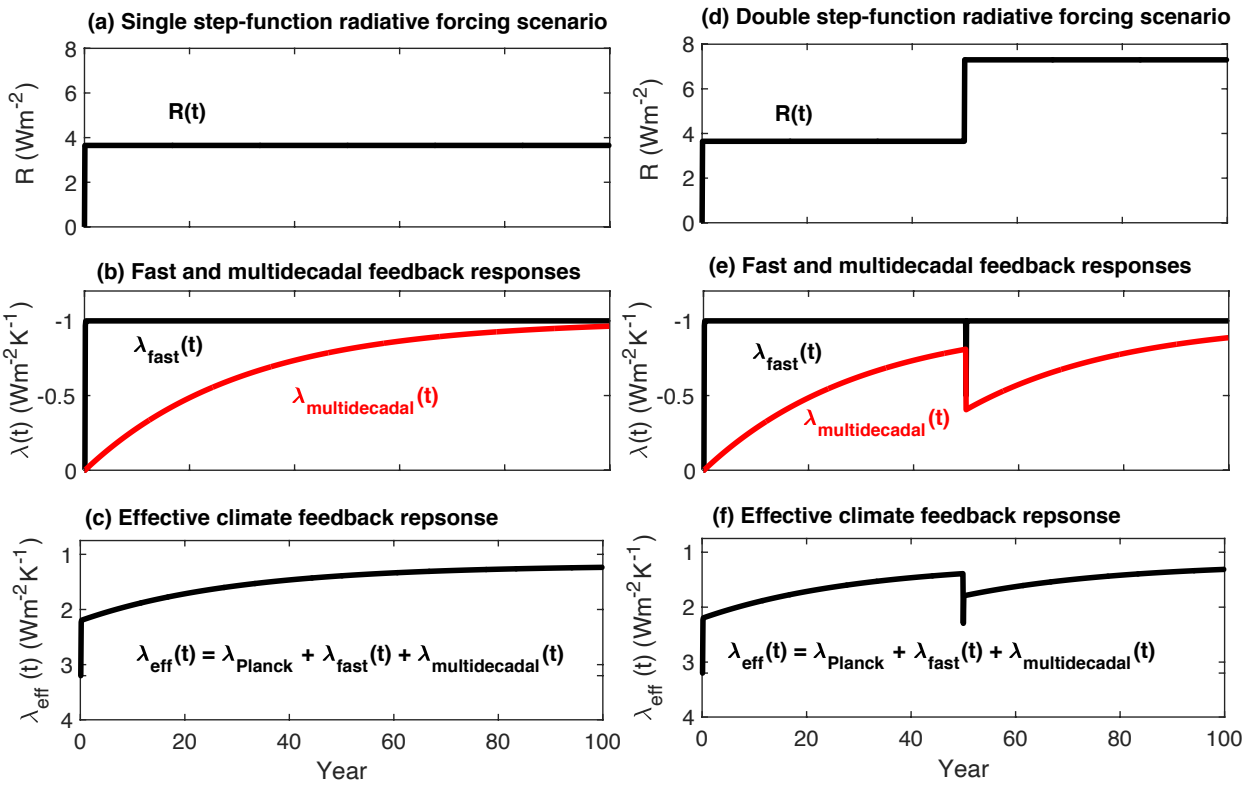

Figure S7: Example climate feedback responses to two idealised step-function radiative forcing scenarios in the WASP model equations. Panels (a), (b) and (c) shows radiative forcing for an idealised single step-function scenarios (a: black). the responses of fast (b: black) and multidecadal (b: red) feedback terms and the overall effective climate feedback response from the Planck, fast and multidecadal feedbacks (c: black). Panels (d), (c) and (f) show the corresponding values for a double step-function idealised radiative forcing. Values of climate feedback terms calculated using equations S8 and S10 with example values used $\lambda_{Planck} = 3.2$ Wm^{-2}K^{-1}; λ_{fast}^{equil} = -1.0 Wm^{-2}K^{-1} ; $\lambda_{multidecadalt}^{equil} = -1.0$ Wm^{-2}K^{-1}; $\tau_{fast} = 10$ days and $\tau_{multidecadal} = 30$ years and using 12 time-steps per year.